AGU PUBLICATIONS

JGR

Journal of Geophysical Research: Atmospheres

RESEARCH ARTICLE
10.1002/2013JD021160

Key Points:
- Significant lightning activity occurs in Western Patagonia
- Lightning storms develop under a cold, weakly unstable postfrontal condition
- Topography and ocean conditions favor lightning activity in Western Patagonia

Correspondence to:
R. D. Garreaud,
rgarreau@dgf.uchile.cl

Citation:
Garreaud, R. D., M. Gabriela Nicora, R. E. Bürgesser, and E. E. Ávila (2014), Lightning in Western Patagonia, *J. Geophys. Res. Atmos.*, *119*, doi:10.1002/2013JD021160.

Received 7 NOV 2013
Accepted 15 MAR 2014
Accepted article online 21 MAR 2014

Lightning in Western Patagonia

René D. Garreaud[1], M. Gabriela Nicora[2], Rodrigo E. Bürgesser[3], and Eldo E. Ávila[3]

[1]Department of Geophysics, Universidad de Chile and Center for Climate and Resilience Research, Santiago, Chile, [2]CEILAP, UNIDEF (MINDEF-CONICET), Buenos Aires, Argentina, [3]FaMAF, Universidad Nacional de Córdoba, IFEG-CONICET, Córdoba, Argentina

Abstract On the basis of 8 years (2005–2012) of stroke data from the World Wide Lightning Location Network we describe the spatial distribution and temporal variability of lightning activity over Western Patagonia. This region extends from ~40°S to 55°S along the west coast of South America, is limited to the east by the austral Andes, and features a hyper-humid, maritime climate. Stroke density exhibits a sharp maximum along the coast of southern Chile. Although precipitation there is largely produced by cold nimbostratus, days with more than one stroke occur up to a third of the time somewhere along the coastal strip. Disperse strokes are also observed off southern Chile. In contrast, strokes are virtually nonexistent over the austral Andes—where precipitation is maximum—and farther east over the dry lowlands of Argentina. Atmospheric reanalysis and satellite imagery are used to characterize the synoptic environment of lightning-producing storms, exemplified by a case study and generalized by a compositing analysis. Lightning activity tends to occur when Western Patagonia is immersed in a pool of cold air behind a front that has reached the coast at ~40°S. Under these circumstances, midlevel cooling occurs before and is more prominent than near-surface cooling, leading to a weakly unstable postfrontal condition. Forced uplift of the strong westerlies impinging on the coastal mountains can trigger convection and produces significant lightning activity in this zone. Farther offshore, large-scale ascent near the cyclone's center may lift near-surface air parcels, fostering shallow convection and dispersing lightning activity.

1. Introduction

Frontal cyclones drifting eastward along the oceanic storm tracks are responsible for most of the precipitation and day-to-day weather variations in the extratropics. These storms are dominated by clouds and precipitation of stratiform nature [e.g., *Houze*, 1993, chapter 9] with rather weak vertical air velocities ($\leq 2\ m\ s^{-1}$). Consistently, they exhibit modest lightning activity relative to deep convective systems over warm land masses. Indeed, global lightning climatologies constructed on the basis of satellite data [e.g., *Christian et al*., 2003] and ground-based networks [*Virts et al*., 2013] reveal that the mean lightning density over the oceans poleward of 40° is 50 to 500 times smaller than the lightning density over tropical/subtropical land masses. The lightning density over extratropical oceans is somewhat larger to the east of North and South America, Japan, and South Africa during their respective winter seasons [e.g., *Virts et al*., 2013, Figure 4], where warm waters prevail and cyclogenesis is frequent [*Hoskins and Hodges*, 2002].

Analyses of specific events over the North Pacific [*Pessi et al*., 2009; *Pessi and Businger*, 2009a] and North Atlantic [*Demetriades and Holle*, 2005] reveal that lightning activity is concentrated along the cold front of midlatitude storms, probably in connection with a line of forced convection known as the narrow cold-frontal rainband [e.g., *Browning*, 1986], as well as near the cyclone's center during its developing stage. *Pessi and Businger* [2009a] also show a consistent logarithmic increase in convective rainfall rates and other storm metrics with increasing lightning rates, opening the possibility of lightning data assimilation to improve numerical weather forecasts over remote ocean regions [*Pessi and Businger*, 2009b]. Lightning has also been reported during cold-season storms over high-latitude, continental regions [*Mäkelä et al*., 2011]. Recently, *Mäkelä et al*. [2013] studied two winter thunderstorms in southern Finland that had adverse effects on aviation. These unseasonable events occurred within the occluded sector of a front, over ice-free sea and with near-zero convective available energy. Thunder during snow storms (the so-called thundersnow events) are infrequent but they have been documented over North America [*Schultz*, 1999; *Market et al*., 2002].

Although winter snow clouds are sometimes as low as 6 km, they can produce lightning and their charge evolution is similar to that on summer thunderstorms [*Takahashi et al*., 1999]. Observations suggest that graupel

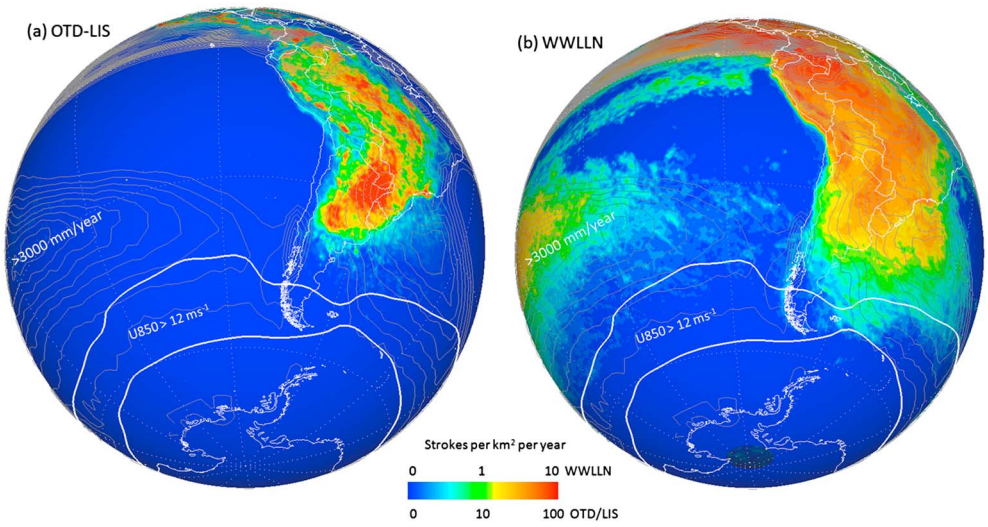

Figure 1. Annual mean frequency of lightning (flashes per km^2/yr) from (a) LIS/OTD and (b) WWLLN. Also shown is annual mean precipitation (grey contours every 300 mm/yr from Climate Prediction Center (CPC) Merged Analysis Precipitation, CMAP) and 850 hPa wind speed in excess of 12 m/s (bounded by white contours, from NCEP-National Center for Atmospheric Research reanalysis) indicative of the SH westerly wind belt and storm track. Vertical perspective (globe view from finite distance).

and ice crystals are the major charge carriers and that noninductive mechanism acts as the main charge separation process in these cold systems. *Ávila et al*. [2013] studied in the laboratory the performance of the noninductive mechanism under microphysical conditions similar to some of those which occur in winter storms. Their results indicate that this mechanism of charge separation may contribute to the electrification processes in the winter thunderstorms, provided that the residence time of the graupel in the cloud is of sufficient duration.

Lightning activity is markedly low (sparse satellite coverage and fewer ground-based receivers to the south of 40°S may exacerbate this condition) along the Southern Hemisphere storm track (Figure 1) that is collocated with the westerly wind belt between 45° and 55°S [e.g., *Hoskins and Hodges*, 2005]. Annual mean rainfall across much of the Southern Oceans is about 1000–1500 mm, but this value changes dramatically as the storm track intercepts Patagonia in the southern tip of South America [e.g., *Garreaud et al*., 2013]. This region extends southward from about 40°S and is divided by the austral Andes (i.e., the southern extent of this mountain range); sea surface temperatures (SSTs) over the adjacent Pacific Ocean do not surpass 10°C. Orographic enhancement upstream of the mountains results in copious precipitation over Western Patagonia (Chilean side). The actual precipitation distribution is poorly constrained, because of the minimum rain gauge network in this extremely inaccessible region, but the annual mean accumulation ranges between 5.000 and 10.000 mm/yr (Figure 2) supporting extensive rainforests, major rivers, and the Northern and Southern Patagonia Ice Fields. Mean precipitation decreases to less than 300 mm/yr just a few tens of kilometers downstream of the continental divide, leading to one of the most dramatic precipitation gradients on Earth [*Smith and Evans*, 2007].

Based on the previous background, conventional wisdom suggests little—if any—lightning activity over the cool, hyper-humid Western Patagonia. Two lines of evidence, however, suggest that lightning in that region does occur rather frequently. First, paleoenvironmental reconstructions based on tree samples and lake sediments have documented significant, albeit variable, wildfire activity over Western Patagonia during the Holocene (see *Holz and Veblen* [2011a] for a review). Before the Euro-Chilean colonization (~ 200 years ago), forest fires in this remote area have been attributed to lightning ignition [*Markgraf and Anderson*, 1994; *Whitlock et al*., 2007] during extended periods of relatively dry and warm conditions [*Holz and Veblen*, 2011b]. Second, the World Wide Lightning Location Network (WWLLN), a ground-based network described in detail in section 2, allows a global, real-time monitoring of lightning activity for ~1700 volcanoes to detect ash cloud lightning signaling an ongoing volcanic eruption (http://wwlln.net/volcanoMonitor.html). The southern Andes hosts more than 33 active volcanoes, but their eruption is rare (e.g., three major events in the last decade (Servicio Nacional de Geologia y Mineria, unpublished report, http://www.sernageomin.cl/volcanes.php).

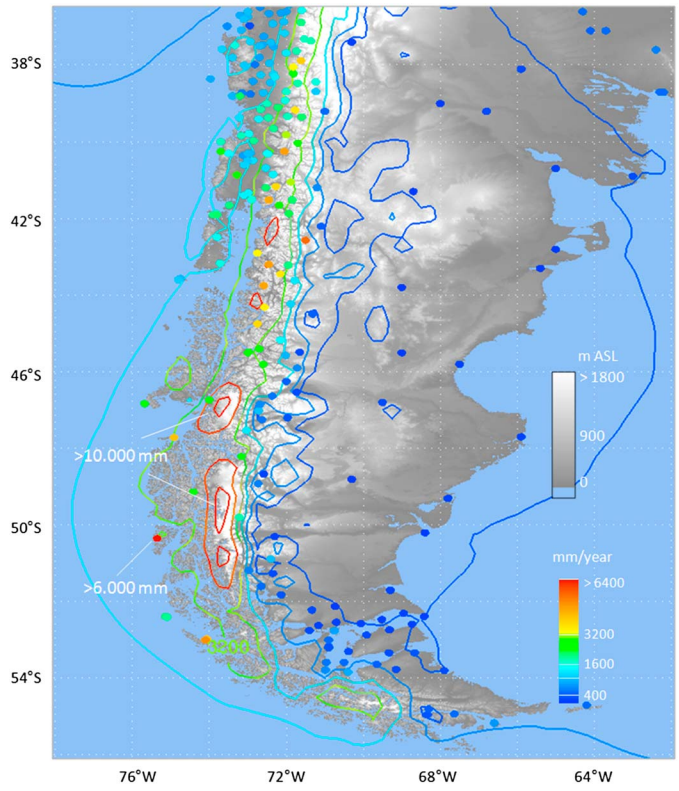

Figure 2. Annual mean precipitation from a regional model simulation (contoured at levels indicated in the color scale) and station data (colored circles, scale at right). The model simulation is PRECIS forced by ERA-40 from 1979 to 2001 (see details in *Garreaud et al.* [2013]). Terrain elevation (gray scale) is from the Shuttle Radar Topography Mission.

In contrast, we noted WWLLN volcanic warnings 4–5 times per month over southern South America that were subsequently interpreted as weather-related events.

In this work we precisely study lightning activity over Western Patagonia, with emphasis in their distribution and attending meteorological conditions. Our study relies on 8 year data from the WWLLN along with other sources of meteorological information described in section 2. The spatial distribution and temporal behavior of the lightning activity is documented in section 3. Section 4 provides a synoptic analysis for the first week of May 2012 when a major lightning event took place over Western Patagonia. A compositing analysis of meteorological conditions is then performed in section 5 to generalize the findings in the case study, along with a consideration of local factors controlling the occurrence of lightning storms. Concluding remarks are presented in section 6, including a conceptual model of Western Patagonia lightning storms.

2. Data

The World Wide Lightning Location Network (WWLLN, http://wwlln.net) started in 2003 with 11 ground-based sensors, and it is currently composed by 70 sensors over all the continents and a few islands [*Hutchins et al.*, 2012; *Virts et al.*, 2013]. The sensors detect very low frequency radio waves (sferics) that are emitted by lightning and travel through the Earth ionosphere waveguide. At least five WWLLN sensors are required to locate a lightning stroke in space and time to within ~5 km and $<$10 μs, respectively, favoring the detection of the most energetic cloud-to-ground strokes [*Abarca et al.*, 2010].

In this work we have used WWLLN data from January 2005 to December 2012, with emphasis on the occurrence of lightning over the Western Patagonia and the adjacent Pacific to the south of ~40°S. The WWLLN detection efficiency (DE) in this region is unknown, and it changed over time (there is no in situ lightning detection network, and the data from the Lightning Imaging Sensor on board of the Tropical Rainfall Measuring Mission satellite are limited to ±38° of latitude), but it is likely between 5 and 10%, the

global efficiency estimated elsewhere [*Lay et al*., 2004; *Abarca et al*., 2010; *Rudlosky and Shea*, 2013]. Based on the energy statistics of the detected strokes, *Hutchins et al*. [2012] further analyzed the *relative* DE of the WWLLN and their change on time. Using their DE model, *Hutchins et al*. [2012] were able to correct the global stroke density for a particular year (2011) leading to major changes over Africa (>50%) but seemingly minor changes over southern South America (<10%) [*Hutchins et al*., 2012, Figure 16].

For our case study (30 April to 3 May 2012) we also used stroke locations derived from the Sferics Timing and Ranging Network (STARNET, see details at http://www.zeus.iag.usp.br/). This network is currently composed by eight ground-based sensors located in Brazil and the adjacent Atlantic (all of them to the north of 25°S) to monitor lightning over the tropical regions. To our knowledge, however, the detection efficiency for STARNET is not available. We have also used historical records of thunderstorm days on a handful of stations in Patagonia compiled by the *World Meteorological Organization* (*WMO*) [1953].

The atmospheric circulation and thermodynamic conditions during lightning-producing storms were characterized using the Climate Forecast System Reanalysis (CFSR) elaborated by the National Centers for Environmental Prediction (NCEP). In this reanalysis, satellite retrievals, surface, and upper air observations are assimilated upon a state-of-the-art numerical model to produce the best estimate of the three-dimensional state of the atmosphere/ocean system. The first version of the reanalysis (CFSRv1) [*Saha et al*., 2010] covers the period 1979–2011, and its second version (CFSRv2) [*Saha et al*., 2014] covers the period from January 2011 until now. A major advantage of CFSR is its much higher spatial resolution relative to other reanalyses; here we used pressure level and surface data available every 6 h on a global $0.5° \times 0.5°$ latitude-longitude grid. The high resolution of CFSR is particularly useful when examining specific storms over Western Patagonia, in conjunction with WWLLN data and visible (channel 1) and thermal infrared (channel 4) satellite images from GOES 13 archived in the NOAA Comprehensive Large Array-data Stewardship System (http://www.class.ncdc.noaa.gov/).

To provide context to our lightning climatology we describe the annual mean precipitation field obtained from several sources. Over land we used the long-term (at least 30 years of data) average values from rain gauges operated by the Chilean weather service and water authority. Because this network has a low density over Western Patagonia, we also employed the results from a 20-yearlong regional climate simulation over southern South America and the adjacent oceans using the PRECIS model [see details and validation in *Garreaud et al*., 2013]. Farther offshore, we used the long-term mean values from the NOAA NCEP Climate Prediction Center Merged Analysis of Precipitation (CMAP) [*Xie and Arkin*, 1997].

3. Spatial and Temporal Distribution

Let us begin our analysis by displaying the lightning density (ρ_L) and the number of days with lightning (N_d) (Figures 3a and 3b). The lightning density is defined here as the count of strokes in nonoverlapping $0.1° \times 0.1°$ latitude-longitude grid boxes considering the whole record (January 2005 to December 2012) divided by 8 years, so it has units of strokes per ~100 km^2/yr. The number of days with lightning is the count of days with a least one stroke in $0.25° \times 0.25°$ latitude-longitude grid boxes considering the whole record divided by 8 years, so it has units of d/yr. The grid box sizes are somewhat arbitrary and do not necessarily coincide with other work's definitions, but they allow us to detect the detailed structure of ρ_L and N_d as well as regional differences.

The ρ_L and N_d maps have a similar, well-defined structure, with a sharp maximum along the Chilean coast from 42° to 52°S (Figure 3). This coastal band of maximum in ρ_L and N_d is collocated with the maximum in precipitation and number of rainy days derived from high-resolution, satellite-based products (the Special Sensor Microwave Imager rain rate estimates) [*Falvey and Garreaud*, 2007, Figure 2] and a local maximum in CFSR convective rainfall rate (not shown). Lightning activity is virtually nonexistent over the austral Andes, including the massive Northern and Southern Patagonia Ice Fields. Very low lightning activity is found over the dry lowlands to the east of the austral Andes, but ρ_L and N_d increase equatorward reaching values comparable to those in Western Patagonia to the north of 38°S. Low stroke density is also observed off southern Chile, but lightning does occur there as shown in Figure 4 by the stroke location for the year 2011. The band of scattered lightning activity over the South Pacific is centered about 3° equatorward of the axis of precipitation maxima, a feature also seen in other storm track regions [*Virts et al*., 2013].

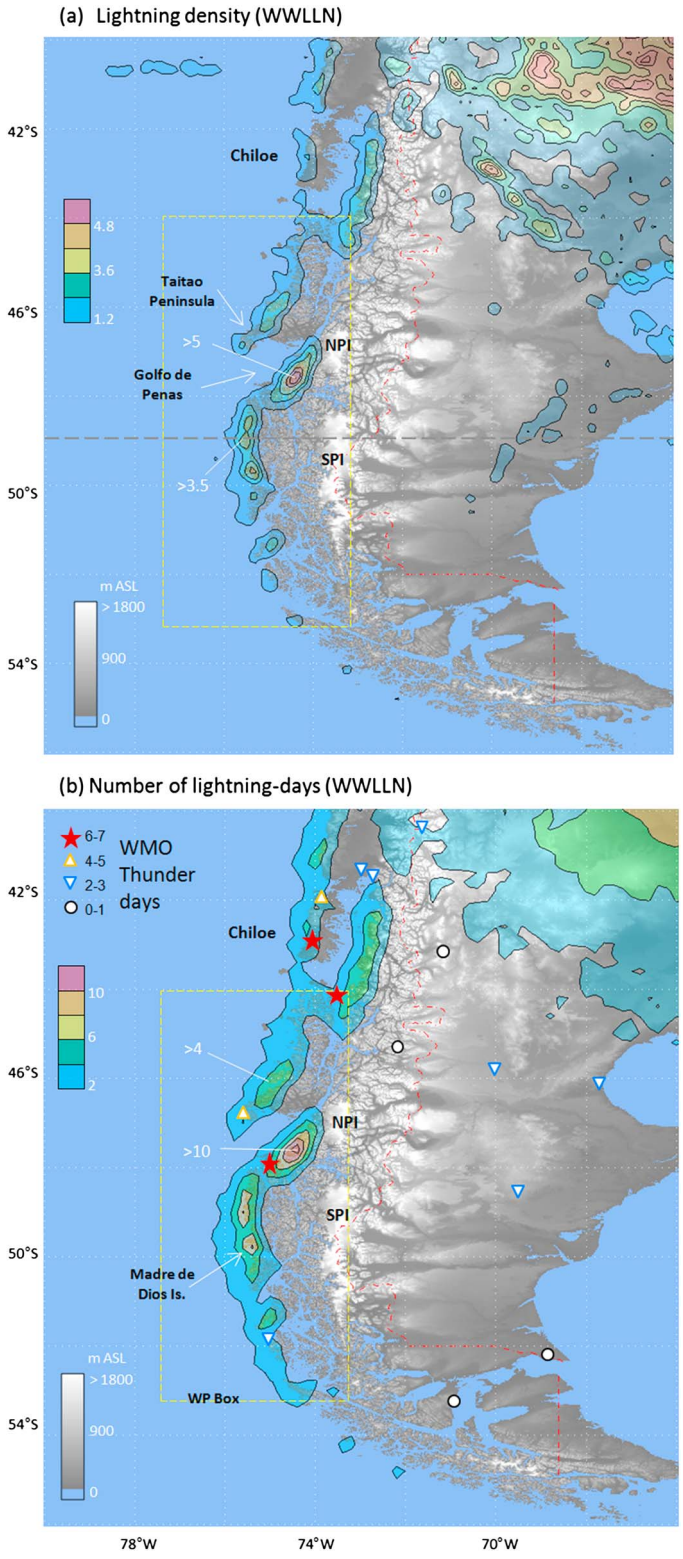

Figure 3. (a) Lightning density contoured every 1.2 stroke in 0.1° × 0.1° latitude-longitude grid boxes per year. (b) Number of lightning days (at least one stroke in 0.25° × 0.25° latitude-longitude grid boxes per year) contoured every 2 d/yr. Data from WWLLN, January 2005 to December 2012. Symbols in Figure 3b are the annual mean number of thunderstorm days from *WMO* [1953]. See text for details. Terrain elevation (gray scale) is from the Shuttle Radar Topography Mission. Also indicated is the Western Patagonia box (yellow rectangle), a zonal transect used in Figure 5, the locations of the Northern and Southern Patagonia Ice Fields, and a few other geographical features. Equirectangular projection is shown.

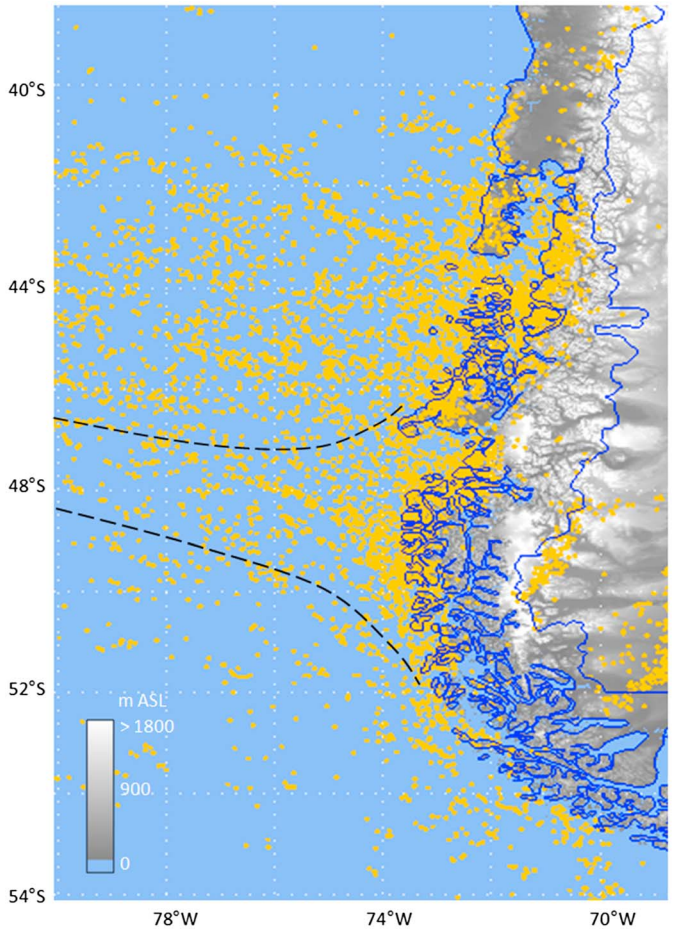

Figure 4. Lightning locations during 2011 (yellow circles) superimposed on the terrain elevation. Data from WWLLN. To avoid excessive overlapping among the circles, the full lightning data over this region were sorted in time and only one every three strokes is plotted (i.e., we are only showing a third of the complete lightning locations). The dashed lines indicate the band of maximum precipitation offshore (from CMAP and PRECIS data, see text). Equirectangular projection is shown.

Granted, the unknown and variable detection efficiency of WWLLN over this region prevents from assigning too much confidence on the *numerical* values of the lightning density (ρ_L) displayed in Figure 3a and our subsequent analyses (Figures 5 and 6). In this exploratory work we have refrained from applying a detection efficiency model to correct the stroke density over Western Patagonia as in *Hutchins et al*. [2012]. Nonetheless, the yearly (2005, 2006,…, 2012) maps of the number of strokes per box normalized by the total number of strokes in Western Patagonia (see below) are very similar and they have a pattern correlation coefficient ≥0.6 for any pair of years, lending confidence to the *spatial pattern* of ρ_L. Moreover, because of its own definition, the values and patterns of N_d are much less affected by any temporal change that may have affected the stroke detection efficiency of the WWLLN [e.g., *Rudlosky and Shea*, 2013].

Further support for the lightning distributions in Figure 3 comes from the survey of thunderstorm days (a day when at least one thunder is heard) presented in *WMO* [1953] on the basis of several years of record. Typically, a thunder is heard by a human observer when it occurs within 20 km from its base station. The annual mean number of thunderstorm days for the available stations is superimposed on the N_d field (Figure 3b), and we note an excellent agreement between these two data sets considering their different nature and temporal coverage.

The lightning maximum along the Chilean coast is nothing but remarkable considering the complex geography of this area, filled with small islands, fiords, embayment, and channels. A closer inspection of Figure 3a shows localized maxima over the seafront of major geographical features, including the islands of

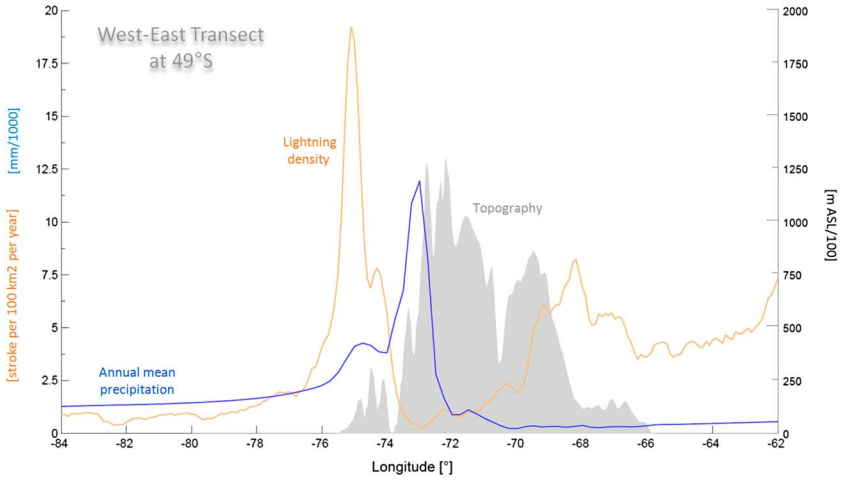

Figure 5. West-east transection at 49°S of the lightning density (yellow line, from WWLLN), annual mean precipitation (blue line, from PRECIS), and terrain elevation (gray area, from Shuttle Radar Topography Mission). Scales for lightning density and precipitation at left and scale for terrain elevation at right.

Madre de Dios (50°S) and Wellington (49°S), the Taitao Peninsula (46.5°S), and the coast of Golfo de Penas (47.5°S), the local maxima for lightning flash density. A zonal transection at 49°S (Figure 5) confirms the lightning's preference for the coastal plains (0–100 m above sea level (asl)) well exposed to the NW winds. Precipitation in these sectors is unknown, but likely around 5000 mm/year, well below the estimated

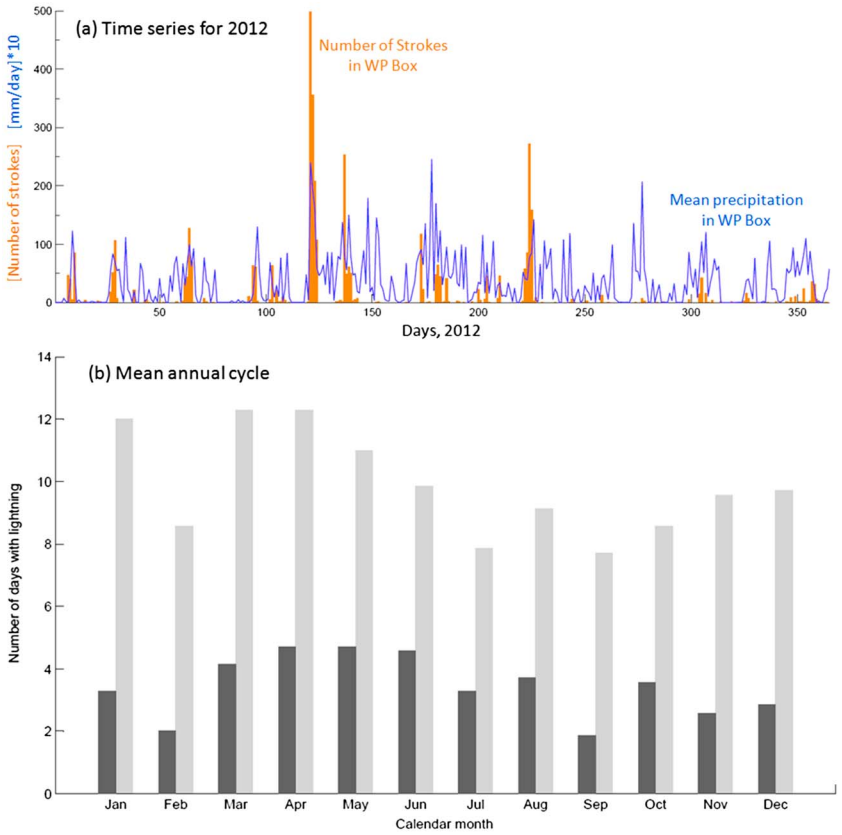

Figure 6. (a) Time series of the number of WWLLN strokes and CFSR total precipitation in the Western Patagonia box (42–54°S/76–70°W, see Figure 3) during year 2012. (b) Black bars: monthly mean (over the 8 year record) number of days with at least one stroke over Western Patagonia box; gray bars: as before but for the monthly mean number of days with at least 10 strokes. Data from WWLLN, January 2005 to December 2012.

Figures 7 and 8 in next page

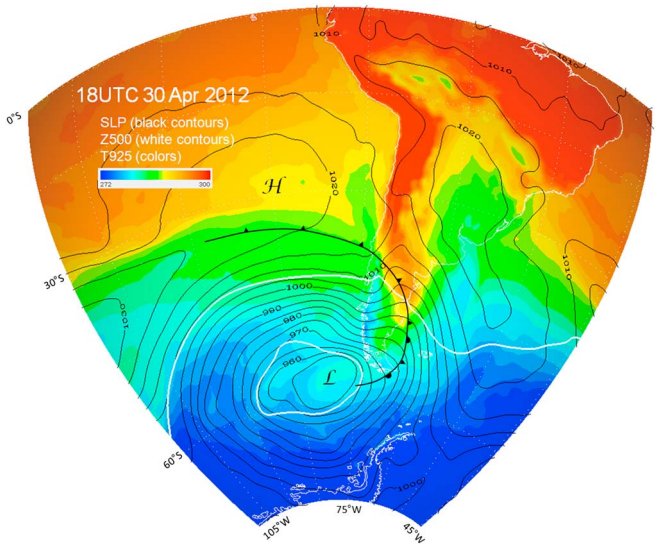

Figure 9. Weather map valid at 1800 UTC 30 April 2012, including SLP (contoured every 5 hPa), 925 hPa air temperature (shading) and 300 hPa geopotential height (5600 and 5500 mgp, white contours). Also indicated is the major cold front rooted in the cyclone (L) over the South Pacific. Data from CFSR.

accumulation over the Patagonia Ice Fields located 50–100 km inland that reach more than 1.5 km asl. A spatial offset between the maximum in lightning activity and the higher terrain maximum has also been found to the west of the Albertine Rift Mountain in central Africa [*Bürgesser et al*., 2013], although it is not as marked as in Western Patagonia.

The temporal behavior of the lighting activity in southern Chile is illustrated by the time series of the daily number of strokes in Western Patagonia box (42–54°S/76–70°W, see Figure 3) for year 2011 (Figure 6a). Recall the dependence of the number of strokes on the WWLLN detection efficiency. Because the strokes are highly clustered on a few spots along the coast, our results are not sensitive to the box definition. During 2011 there were 125 lightning days in Western Patagonia; other years show a similar behavior (not shown), and the yearly number of lightning days in the Western Patagonia box varies from 107 in 2008 to 151 in 2012, possibly as a consequence of changes in the detection efficiency and natural variability. Lightning activity concentrates in events of 1–4 day duration recurring a few times per month. Figure 6a also includes CFSR total precipitation over the Western Patagonia box which is highly recurrent there (nearly 70% of the time); lightning days are accompanied by precipitation all the time but there are many precipitation days with no lightning.

Using the 8 year record, the monthly average number of lightning days (as well as days with more than 10 strokes) in the Western Patagonia box is shown in Figure 6b. Consistent with a small thermal forcing at high latitudes, the lightning activity in Western Patagonia exhibits a weak annual cycle. Lightning activity, however, tends to be more frequent from summer in the Southern Hemisphere (SH) (December, January, and February) to late fall, peaking in March to April, and somewhat lower in late winter and spring (see also Figure 6a). Likewise, the number of station-based thunderstorm days in Western Patagonia is slightly larger in summer and fall [*WMO*, 1953]. We also verified that the lightning density pattern in every month and season is very similar to the annual map (Figure 3), with a sharp maximum in lightning activity along the Western Patagonia coast where strokes occur in nearly a third of days.

4. A Case Study

Nearly 500 strokes were detected within the Western Patagonia box on 30 April 2012 (most of them after noon), the maximum daily count on record. Significant lightning activity continued until 3 May (Figure 7a) with a total of 900 strokes during this event. Figure 8 shows the location of the lightning (from both WWLLN and STARNET) during 30 April. The lightning distribution for that day followed the climatological pattern

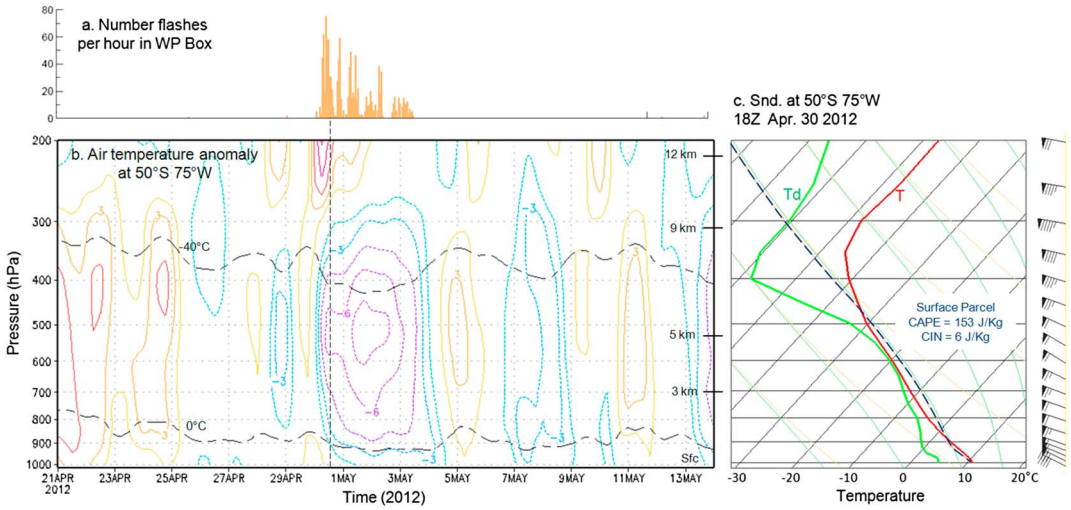

Figure 7. Selected meteorological variables during a major lightning storm in Western Patagonia. (a) Number of WWLLN strokes per hour in the Western Patagonia box from April 21 to May 13, 2012. The strokes concentrated in the afternoon of April 30 and continued until May 3. (b) Time-height diagram of the air temperature anomaly at 50°S 75°W (Golfo de Penas). The anomalies were calculated subtracting the seasonal mean from the 6-hr data at each level. (c) Sounding over Golfo de Penas at 18Z April 30, 2012 (time of maximum lightning activity). Panels (b) and (c) were constructed using CFSR data.

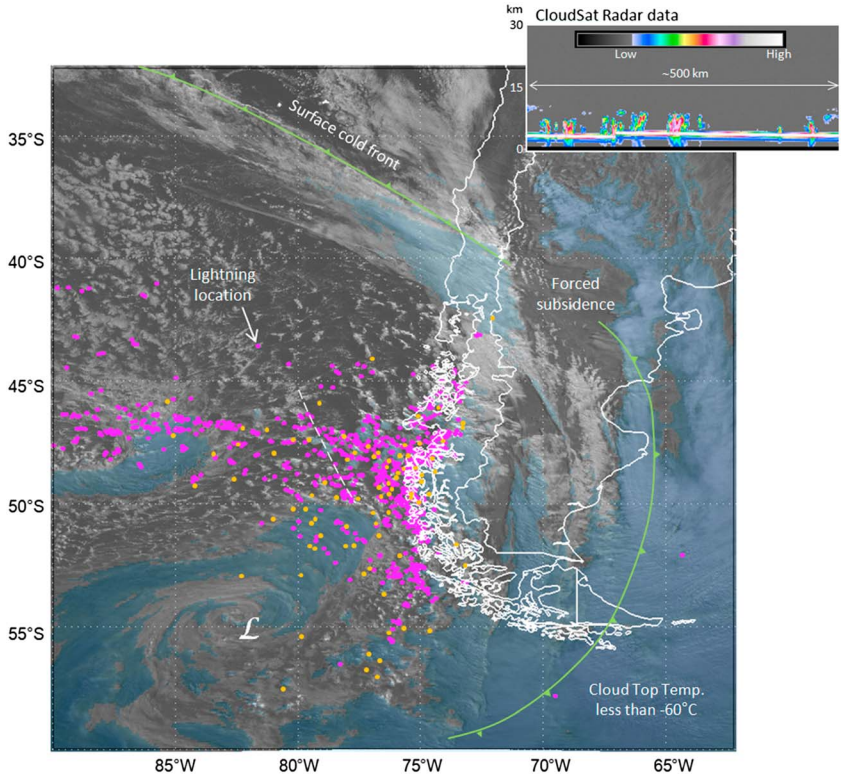

Figure 8. Main panel: Stroke locations from WWLLN (purple circles) and Startnet (orange circles) during the afternoon of April 30, 2012, superimposed on the GOES-13 visible image at 1745 UTC of that day. The faint blue shading indicates cloud top temperatures lower than -60°C derived from the concurrent GOES-13 infrared (IR2) image. Also indicated is the position of a cold front land falling in southern Chile. Inset: Quick look image from the CloudSat radar data along the transect in white, dashed line in the main map for 18 18 UTC May 1, 2012.

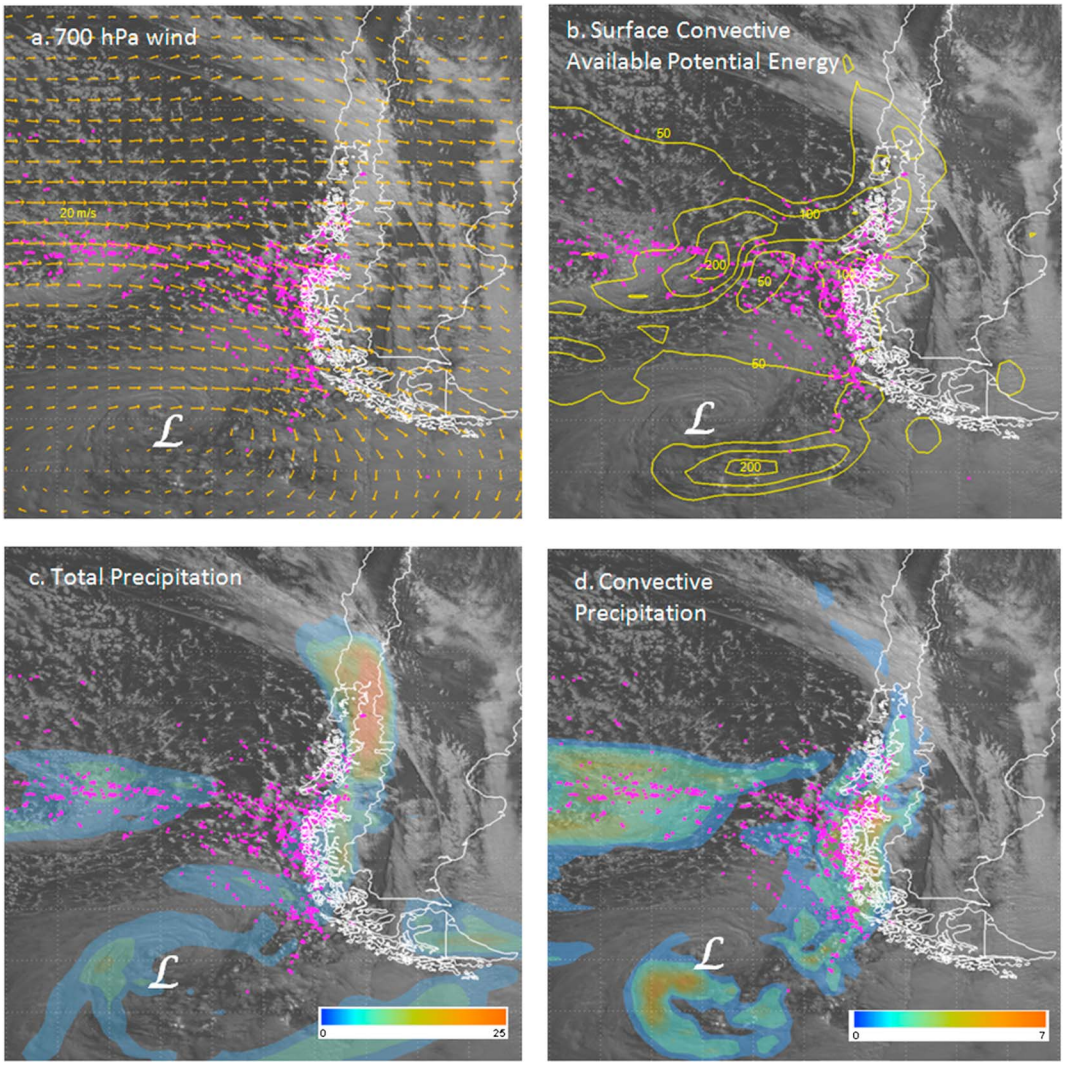

Figure 10. Selected CFSR meteorological fields for 30 April 2012, at 1800 UTC, superimposed on the GOES 13 visible image and WWLLN stroke locations (purple circles) during the afternoon of that day. (a) 700 hPa wind vectors. The longest arrows are 20 m/s. (b) Surface CAPE contoured every 50 J/kg. (c) Total precipitation accumulated during the last 6 h (scale at bottom). (d) Convective precipitation accumulated during the last 6 h (scale at bottom). In each panel the letter L indicates the cyclone's center. Equirectangular projection is shown.

(cf. Figures 8 and 3) with most strokes clustered along the coast of southern Chile, disperse strokes offshore, and no strokes over the austral Andes or farther east. We also note a general agreement in the stroke locations between both data sets, although WWLLN detected 5 times more strokes than STARNET.

Important meteorological features of this event are revealed by the composited GOES image (1745 UTC of 30 April, Figure 8) together with the concurrent weather map (Figure 9). A key ingredient is a deep cyclone (central pressure $<$ 955 hPa) to the west of the tip of the continent, driving strong low-level westerly flow over the South Pacific (Figure 10a; see also the wind profile in Figure 7c). A closed low is also seen in the 500 hPa geopotential height right above the surface cyclone (Figure 9), indicative of the mature stage of this system. The attending cold temperatures in the middle troposphere moved eastward from the central Pacific on 27 April to reach the west coast on 30 April and remained stationary there for the next 4 days (not shown).

Cold air advection maintained a cold front over the South Pacific, evident in the temperature analysis and satellite imagery, intercepting the Chilean coast at about 38°. The front is interrupted to the east of the Andes but reformed near the Atlantic sea border spiraling toward the cyclone center. The total precipitation (stable + convective, Figure 10c) maximized in the sector where the cold front land fell (up to 25 mm in 6 h)

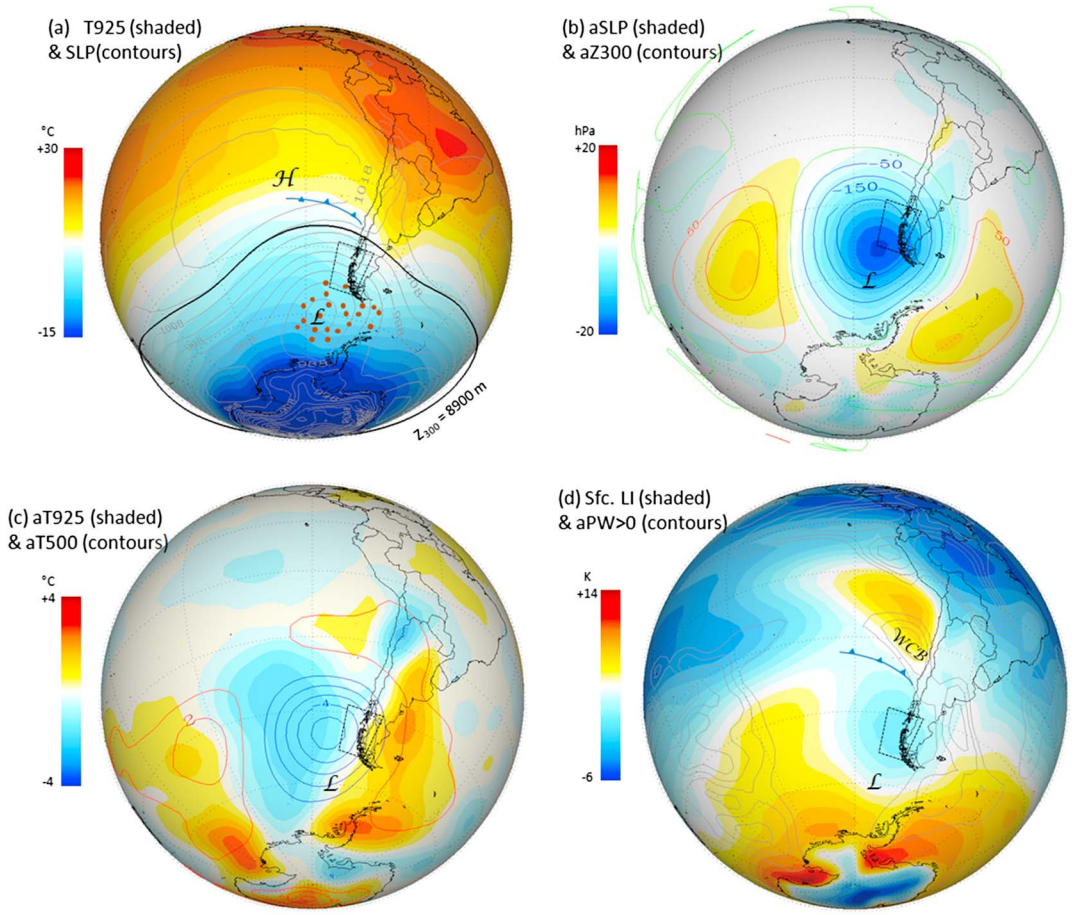

Figure 11. Composite maps of selected CFSR meteorological fields for the 90 days with more than 50 strokes in the Western Patagonia box (dashed box). (a) Sea level pressure (SLP) contoured every 5 hPa and 925 hPa air temperature (shaded, scale at left). Also indicated is the cyclone's core for selected cases (red dots) and the most common location of the cold front over the southeast Pacific. (b) SLP anomalies (shaded, scale at left) and 300 hPa geopotential height anomalies (contoured every 50 mgp). Anomalies are calculated as departure from the long-term mean. (c) The 925 hPa air temperature anomalies (shaded, scale at left) and 500 hPa air temperature anomalies (contoured every 1°C). (d) Surface lifted index (shaded, scale at left) and precipitable water anomaly (contoured at 5, 10, 15, and ≥20 cm). The letter L indicates the average cyclone center, and WCB is the mean location of the warm conveyor belt. Shown is the vertical perspective (globe view from finite distance).

and was also large over the mountains down to 45°S because of the marked orographic enhancement. Notably, lightning activity did not occur along the cold front, but it was found within the cold, postfrontal air mass that had reached Western Patagonia. Open cell clouds are evident in the satellite image within the postfrontal sector off Western Patagonia, and there is a hint of a developing polar low farther west (47°S–87°W) accompanied by some lightning activity as well. The raw echo return power from a CloudSat quick look image (inset in Figure 8) further reveals the shallow nature of the postfrontal convection with cloud tops below ~7 km asl. Also note that convective precipitation was a minor contribution over the frontal sector and the austral Andes, but it dominates over the postfrontal sector (~5 mm in 6 h, Figure 10d) where lightning occurred.

The time-pressure diagram of the air temperature anomalies (Figure 7b) shows the differential cooling at low and midlevels off Western Patagonia during the development of this event. In the middle troposphere there was a rapid cooling right at the beginning of the event (30 April) in connection with the arrival of the postfrontal air mass. The cooling continued until 2 May, when 500 hPa air temperatures were 10°C cooler than the seasonal average. The cooling below 900 hPa was weaker (less than 3°C) and took place more gradually than aloft because of the sensible heat flux (~80 W m^{-2}) at the sea surface. Thus, the most unstable condition off Western Patagonia occurred on 30 April, 12–24 h after the passage of the cold front. Indeed, convective available

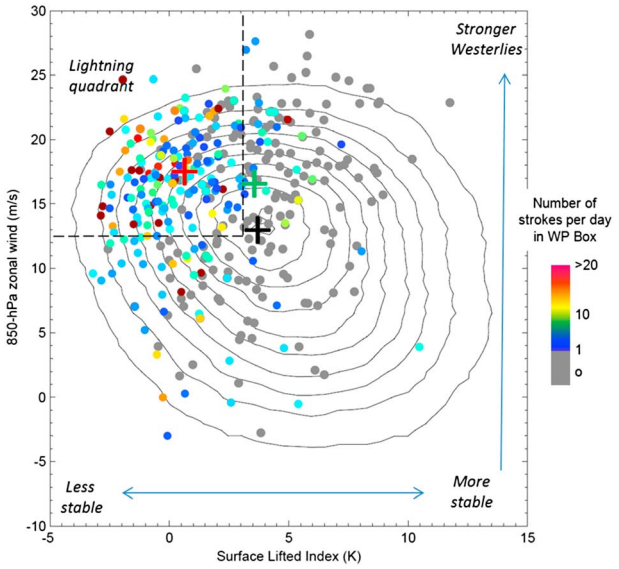

Figure 12. Joint distribution of the daily mean surface lifted index (LI, horizontal axis) and 850 hPa zonal wind (U850, vertical axis) over the Western Patagonia box (see Figure 3) considering all days from January 2005 to December 2012. The isolines of frequency are drawn every 2%, and the full-sample average is indicated by a black cross. The gray circles are the daily values of LI-U850 for those days with more than 10 mm in the Western Patagonia box; the subsample mean is indicated by a green cross. The color circles are the daily values of LI-U850 for those days with more than one WWLLN strokes over Western Patagonia box; the subsample mean is indicated by a red cross. The color of these circles indicates the number of strokes: warm colors indicate more strokes and cold colors indicate less strokes.

potential energy (CAPE) values of about 150 J/kg and negative lifted index (LI) are seen across much of the postfrontal sector during the period of intense lightning activity (Figure 10d).

A sounding (from CFSR data) at Golfo de Penas (50°S, 75°W) for the time of maximum stroke occurrence further illustrates the thermal structure of the postfrontal air mass (Figure 7c). Near-surface air temperature was about 10°C, the freezing level was at ~1300 m asl, and the −40°C isotherm was at ~6500 m asl. Saturation was observed in the lower troposphere capped by a layer of dry air above 500 hPa. More importantly, an air parcel lifted from the surface reaches its level of free convection at only 1000 m asl and its level of neutral buoyancy at 5500 m asl, so there was a very small value of Convective Inhibition (< 10 J/kg), a modest value of CAPE (156 J/kg) and slightly negative values of the LI (−0.2°C).

5. Climatological Analysis

5.1. Large-Scale Composites

A cursory inspection of the weather maps and satellite imagery for several cases of significant lightning activity in Western Patagonia reveals a synoptic environment similar to that documented in our case study. These conditions are synthesized here using a compositing analysis of selected meteorological fields for the 90 days on record with more than 50 strokes in the Western Patagonia box. The lightning distribution for this subsample of days follows the full-sample spatial pattern (not shown).

The composite maps of sea level pressure (SLP) and 925 hPa air temperature (Figure 11a) show a low-pressure center west of the Drake Passage and the incursion of cold air over the southeast Pacific extending along the Chilean coast up to ~40°S. The location of the composite low-pressure area (very close to the cyclone position in the case study) reflects that nearly all the lightning-producing storms in Western Patagonia were associated with a deep low over the southeast Pacific (also note the cyclone's central position for selected cases). Likewise, a cold front making landfall *to the north* of Western Patagonia was a highly common feature of these storms, evidenced in our composite analysis by a baroclinic zone in the low-level air temperature (Figure 11a) and a tongue of moist air ahead of the front in the map of precipitable water anomalies (Figure 11d). Thus, significant lightning activity in Western Patagonia most often occurs as the postfrontal air mass has reached this region. Figure 11b shows the composite anomalies of SLP and the 300 hPa geopotential height. Negative anomalies are collocated just west of the tip of the continent, indicative of the barotropic structure, mature stage of the midlatitude cyclone that drifted slowly eastward.

Negative temperature anomalies in the middle and lower troposphere (Figure 11c) are also located off Western Patagonia. Along the coast of southern Chile the composite 500 hPa cooling is much larger (~4°C) than the cooling at low levels (<1°C), leading to the development of a broad area of convective instability in the postfrontal air mass that encompasses Patagonia and the adjacent Pacific. To illustrate such unstable

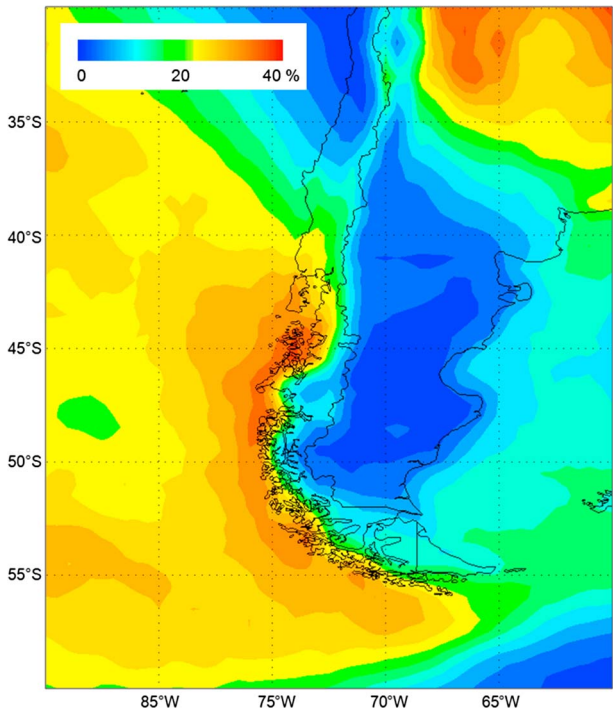

Figure 13. Annual mean frequency of the surface lifted index (LI) of less than 0.5°C over southern South America. Note the high frequency (over 30% of the time) with weakly unstable convective conditions off Western Patagonia. Data from CFSR (2005–2012). Equirectangular projection is shown.

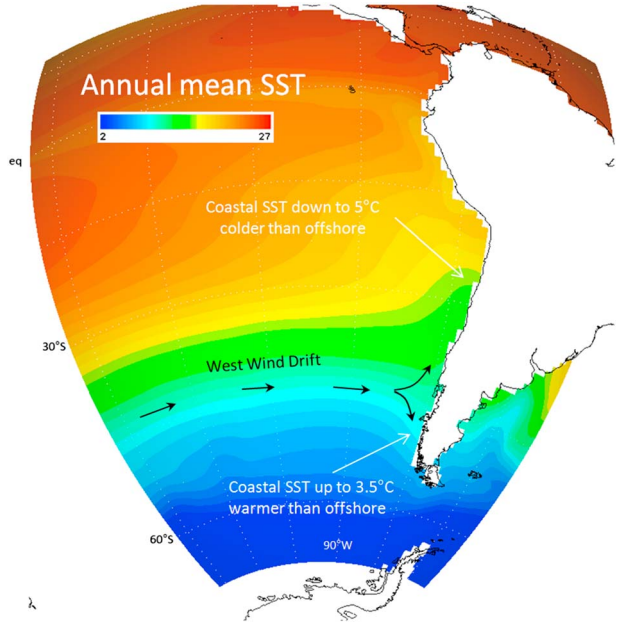

Figure 14. NCEP optimally interpolated annual mean sea surface temperature over the eastern Pacific. Note how the zonal symmetry over open ocean breaks down along the Chilean coast, especially off Western Patagonia. Vertical perspective (globe view from finite distance).

conditions Figure 11d shows the composite map of the surface lifted index (LI) with near-zero values over Western Patagonia and offshore. We choose the lifted index given its normal distribution, more suitable for the compositing analysis, but other stability indices show a similar pattern (e.g., CAPE; not shown). It is within this weakly unstable region where most lightning occur.

5.2. Local Control

Our case study and compositing analysis suggest that both weak instability in the lower troposphere (e.g., nonzero CAPE near-zero lifted index) and strong low-level westerly flow characterize the local environment during lightning storms in Western Patagonia. To generalize these results, let us examine the joint distribution of the daily lifted index (LI) and the 850 hPa zonal wind speed (U850) averaged over the Western Patagonia box (Figure 12). When considering the full sample (every day from 2005 to 2012) the joint distribution (shown by isolines of frequency) is approximately binormal, although positively skewed for both LI and U850, with central values (mean ± standard deviation) of 5.0 ± 3.2°C and 11.2 ± 3.2 m s^{-1}, respectively.

The subsample of days with more than 10 mm of precipitation (rainy days) tends to occur with stronger than average zonal flow (16.2 ± 2 m s^{-1}) consistent with [*Garreaud et al.*, 2013, their Figure 5] that documented a strong correlation between rainfall and zonal wind aloft, upstream of the extratropical Andes. In contrast, rainy days occur under the full range of LI, and the subsample average (3.7 ± 2.6°C) is just slightly lower than the full-sample average.

The subsample of lightning days (more than one lightning in Western Patagonia) is concentrated in the upper left quadrant of the

LI-U850 frequency distribution: lightning days tend to occur under stronger than average low-level westerlies ($16.5 \pm 2\ m\ s^{-1}$) and much lower than average LI ($0.7 \pm 1.3°C$). The stability control on lightning activity is tighter than the zonal flow control: about 15% of the lightning days occur with rather weak flow (less than 13 m/s), but almost no lightning days occur when LI is larger than 5°C. There is also a positive, albeit weak, logarithmic relationship between stability and the number of lightning at daily time scales over Western Patagonia, consistent with the findings by *Pessi and Businger* [2009a] over the North Pacific.

The control that stability exerts on lightning activity also occurs spatially. Figure 13 displays the frequency of days with LI ≤ 0.5°C (roughly equivalent to CAPE ≥ 50 J/kg) over southern South America, a modest value for convection but low enough to trigger lightning over Western Patagonia. The largest frequencies (about 30%) in the extratropics are found along the coast of southern Chile, decaying gradually offshore and sharply inland, matching perfectly with the region of high lightning activity in Western Patagonia (cf. Figures 3 and 13). Recall that unstable conditions in this region are associated with a transient cooling that increases upward under the synoptic conditions identified before. The coastal area of Western Patagonia also exhibits a local maximum in precipitation (as detected by microwave satellite estimates) [*Falvey and Garreaud*, 2007] and convective rainfall rates from CFSR (not shown).

The coastal confinement of the area of frequent near-zero LI observed in Figure 13 is rather puzzling. The occurrence of intense cold anomalies at midlevels should be as frequent in the coastal area as offshore, so that near-surface conditions must play a key role. As noted before, cold SSTs are found along the west coast of South America. Nevertheless, the west wind drift—a surface current across much of the Pacific—intercepts the continent at about 48°S leading to a poleward current and coastal downwelling off Western Patagonia [*Neshyba and Fonseca*, 1980]. Consequently, SSTs in the near-shore region are 3–4°C warmer than offshore (Figure 14), producing the most favorable conditions for instability buildup than anywhere else in the southeast Pacific.

6. Conceptual Model and Concluding Remarks

Eight years of global stroke detection from the WWLLN has allowed to identify a maximum of lightning activity over Western Patagonia (42°–52°S), a cool, hyper-humid region located just downstream of the South Pacific storm track and bounded to the east by the austral Andes. Cloud electrification is not expected in this region given the predominance of stable, deep stratiform precipitation there, but days with at least one stroke occur up to a third of the time along the coast, being slightly more frequent during late summer and fall.

Lightning-producing storms last 1–3 days and develop under a recurrent synoptic environment identified in a case study and generalized by a compositing analysis of 90 events. A key ingredient is a deep surface cyclone over the South Pacific, Drake Passage, often below a closed upper level low pressure, indicative of the mature stage of the disturbance. By the day of significant lightning activity the attending cold front has reached the coast of southern Chile at about 40°S so that Western Patagonia is immersed in the postfrontal sector of the system. During these subantarctic air incursions, the cooling above 700 hPa occurs before and is more pronounced than the cooling at lower levels, leading to a weakly unstable environment off the coast of southern Chile (CAPE ~ 100 J/kg; LI ~ 0°C). Most of the strokes are located right along the coast, and some strokes occur offshore where shallow, open cell clouds are readily identifiable and convective rainfall dominates. In contrast, few (or no) strokes are observed along the cold front or the austral Andes where the precipitation maximizes.

We interpret this conspicuous spatial structure as follows. Under the weakly unstable conditions that prevail in the postfrontal air mass, large-scale ascent near the cyclone's center may lift near-surface air parcels over open ocean fostering shallow convection and disperse lightning activity. Near the coast a second ingredient comes into play. The moderate to strong westerly flow impinges over the coastal mountains that rise sharply to 300–700 m asl, forcing a rapid uplift of the marine air that trigger convection and produces significant lightning activity. Forced accent continues farther inland but the cold, ice-covered surface precludes the development of convection. Clearly, in situ measurements (e.g., coastal radiosondes) are much necessary to validate this conceptual model. Furthermore, the numerical values of lightning density in this region are dependent on the WWLLN detection efficiency, which is variable and unknown over this region due to lack of independent measurements. By the contrary, the spatial pattern of the lightning density as well as the number of days with lightning appears more robust.

In addition to the prominent coastal topography, the confinement of significant lightning activity off Western Patagonia seems also associated with the surface boundary conditions over the adjacent Pacific. Although cold SST (<10°C) prevails year round, these offshore waters are up to 3°C warmer than those over open ocean producing the most favorable conditions for instability buildup than anywhere else in the southeast Pacific when an midlevel cold anomaly passes over. The relatively warm coastal waters are due to the coastal downwelling and poleward flow generated by the West Wind Drift. Therefore, seasonal, interannual, and longer time fluctuations in the intensity and position of this current may modulate changes in the lightning activity in Western Patagonia.

Acknowledgments

The authors wish to thank the World Wide Lightning Location Network (http://wwlln.net), collaboration among over 60 universities and institutions, for providing the lightning location data used in this paper. The manuscript was improved considerably through the comments and suggestions by three anonymous reviewers. R.G. was supported by FONDECYT-Chile (grant 1110169) and FONDAP/CONICYT Chile (grant 15110009-CR2). This work was supported by SECYT-UNC, CONICET and FONCYT, and PIDDEF 14/12, MINDEF Argentina.

References

Abarca, S. F., K. L. Corbosiero, and T. J. Galarneau Jr. (2010), An evaluation of the Worldwide Lightning Location Network (WWLLN) using the National Lightning Detection Network (NLDN) as ground truth, *J. Geophys. Res.*, *115*, D18206, doi:10.1029/2009JD013411.

Ávila, E. E., R. A. Lighezzolo, N. E. Castellano, R. G. Pereyra, and R. E. Bürgesser (2013), Laboratory measurements of charge separation in low liquid water content conditions and low impact velocity, *J. Geophys. Res. Atmos.*, *118*, 6680–6687, doi:10.1002/jgrd.50555.

Browning, K. A. (1986), Conceptual models of precipitation systems, *Weather Forecasting*, *1*, 23–41.

Bürgesser, R. E., M. G. Nicora, and E. E. Ávila (2013), Spatial and time distribution of the flash rate over tropical Africa, *J. Atmos. Sol. Terr. Phys.*, *94*, 41–48.

Christian, H. J., R. J. Blakeslee, D. J. Boccippio, W. L. Boeck, D. E. Buechler, K. T. Driscoll, S. J. Goodman, J. M. Hall, W. J. Koshak, and D. M. Mach (2003), Global frequency and distribution of lightning as observed from space by the Optical Transient Detector, *J. Geophys. Res.*, *108*(D1), 4005, doi:10.1029/2002JD002347.

Demetriades, N. W., and R. L. Holle (2005), Lightning produced by cold season extratropical cyclones: Observations related to nowcasting storm development, intensity and precipitation amounts, Conference on Meteorological Applications of Lightning Data; AMS; Tucson, Ariz.

Falvey, M., and R. Garreaud (2007), Wintertime precipitation episodes in central Chile: Associated meteorological conditions and orographic influences, *J. Hydrometeorol.*, *8*, 171–193.

Garreaud, R., P. Lopez, M. Minvielle, and M. Rojas (2013), Large-scale control on the Patagonian climate, *J. Clim.*, *26*, 215–230.

Holz, A., and T. T. Veblen (2011a), The amplifying effects of humans on fire regimes in temperate rainforests in Western Patagonia, *Palaeogeogr. Palaeoclimatol. Palaeoecol.*, *311*, 82–92.

Holz, A., and T. T. Veblen (2011b), Variability in the southern annular mode determines wildfire activity in Patagonia, *Geophys. Res. Lett.*, *38*, L14710, doi:10.1029/2011GL047674.

Hoskins, B. J., and K. I. Hodges (2002), New perspectives on the Northern Hemisphere winter storm tracks, *J. Atmos. Sci.*, *59*, 1041–1061.

Hoskins, B. J., and K. I. Hodges (2005), A new perspective on Southern Hemisphere storm tracks, *J. Clim.*, *18*, 4108–4129.

Houze, R. A., Jr. (1993), *Cloud Dynamics*, vol. 53, 523 pp., Elsevier, San Diego, Calif.

Hutchins, M., R. Holzworth, J. Brundell, and C. Rodger (2012), Relative detection efficiency of the world wide lightning location network, *Radio Sci.*, *47*, RS6005, doi:10.1029/2012RS005049.

Lay, E. H., R. H. Holzworth, C. J. Rodger, J. N. Thomas, O. Pinto Jr., and R. L. Dowden (2004), WWLLN global lightning detection system: Regional validation study in Brazil, *Geophys. Res. Lett.*, *31*, L03102, doi:10.1029/2003GL018882.

Mäkelä, A., P. Rossi, and D. M. Schultz (2011), The daily cloud-to-ground lightning flash density in the contiguous United States and Finland, *Mon. Weather Rev.*, *139*, 1323–1337.

Mäkelä, A., E. Saltikoff, J. Julkunen, I. Juga, E. Gregow, and S. Niemelä (2013), Cold-season thunderstorms in Finland and their effect on aviation safety, *Bull. Am. Meteorol. Soc.*, *94*, 847–858.

Market, P. S., C. E. Halcomb, and R. L. Ebert (2002), A climatology of thundersnow events over the contiguous United States, *Weather Forecasting*, *17*, 1290–1295.

Markgraf, V., and L. Anderson (1994), Fire history of Patagonia: Climate versus human cause, *Rev. Inst. Geol.*, *15*, 35–47.

Neshyba, S., and T. R. Fonseca (1980), Evidence for counterflow to the west wind drift off South America, *J. Geophys. Res.*, *85*(C9), 4888–4892.

Pessi, A. T., and S. Businger (2009a), Relationships among lightning, precipitation, and hydrometeor characteristics over the North Pacific Ocean, *J. Appl. Meteorol. Climatol.*, *48*, 833–848.

Pessi, A. T., and S. Businger (2009b), The impact of lightning data assimilation on a winter storm simulation over the North Pacific Ocean, *Mon. Weather Rev.*, *137*, 3177–3195.

Pessi, A. T., S. Businger, K. Cummins, N. Demetriades, M. Murphy, and B. Pifer (2009), Development of a long-range lightning detection network for the Pacific: Construction, calibration, and performance, *J. Atmos. Oceanic Technol.*, *26*, 145–166.

Rudlosky, S. D., and D. T. Shea (2013), Evaluating WWLLN performance relative to TRMM/LIS, *Geophys. Res. Lett.*, *40*, 2344–2348, doi:10.1002/grl.50428.

Saha, S., S. Moorthi, H.-L. Pan, X. Wu, J. Wang, S. Nadiga, P. Tripp, R. Kistler, J. Woollen, and D. Behringer (2010), The NCEP climate forecast system reanalysis, *Bull. Am. Meteorol. Soc.*, *91*, 1015–1057.

Saha, S., S. Moorthi, X. Wu, J. Wang, S. Nadiga, P. Tripp, H.-L. Pan, D. Behringer, Y.-T. Hou, and H.-Y. Chuang (2014), The NCEP climate forecast system version 2, *J. Clim.*, *27*, 2185–2208, doi:10.1175/JCLI-D-12-00823.1.

Schultz, D. M. (1999), Lake-effect snowstorms in northern Utah and Western New York with and without lightning, *Weather Forecasting*, *14*, 1023–1031.

Smith, R., and J. Evans (2007), Orographic precipitation and water vapor fractionation over the southern Andes, *J. Hydrometeorol.*, *8*, 3–19.

Takahashi, T., T. Tajiri, and Y. Sonoi (1999), Charges on graupel and snow crystals and the electrical structure of winter thunderstorms, *J. Atmos. Sci.*, *56*, 1561–1578.

Virts, K. S., J. M. Wallace, M. L. Hutchins, and R. H. Holzworth (2013), Highlights of a new ground-based, hourly global lightning climatology, *Bull. Am. Meteorol. Soc.*, *94*, 1381–1391, doi:10.1175/BAMS-D-12-00082.1.

Whitlock, C., P. I. Moreno, and P. Bartlein (2007), Climatic controls of Holocene fire patterns in southern South America, *Quat. Res.*, *68*, 28–36.

World Meteorological Organization (1953), World distribution of thunderstorm days. Part I: Tables. Geneve, 213 pp.

Xie, P., and P. A. Arkin (1997), Global precipitation: A 17-year monthly analysis based on gauge observations, satellite estimates, and numerical model outputs, *Bull. Am. Meteorol. Soc.*, *78*, 2539–2558.